Charge carrier transport in poly(*p*-phenylenevinylene) light-emitting devices

S. Forero, P. H. Nguyen, W. Brütting* and M. Schwoerer

Experimentalphysik II, Universität Bayreuth, 95440 Bayreuth, Germany.
E-mail: wolfgang.bruetting@uni-bayreuth.de

The role of doping and trap states for charge carrier transport in light-emitting devices based on unsubstituted poly(*p*-phenylenevinylene) (PPV) was investigated and charge carrier mobilities were determined by different techniques. Using temperature dependent impedance spectroscopy and thermally stimulated currents, the energetic depth and density of states created by doping of PPV during device fabrication on different substrate materials were determined. It was found that the conversion of PPV on indium–tin oxide (ITO) substrates creates shallow traps with a depth of about 0.1–0.2 eV, which are responsible for the p-type doping of PPV and govern the room temperature device characteristics. The total density of ionized acceptors at room temperature is of the order of 10^{16}–10^{17} cm^{-3}. The temperature dependent behaviour of electrical transport quantities such as conductivity and mobility is dominated by deeper states with energies in the range 0.6–1 eV. Their density can be varied by applying a vacuum to the devices. The charge carrier mobility in PPV was determined by the time-of-flight (TOF) method on devices with the configuration ITO/PPV/Al, which is typically used in light-emitting diodes. Hole mobilities in the region of 10^{-5} cm^2 V^{-1} s^{-1} at room temperature for an electric field of about 10^5 V cm^{-1} were obtained. Field and temperature dependent TOF measurements yielded an exponential increase in the mobility with increase in the applied field and thermally activated behaviour with activation energies between 0.4 and 0.7 eV on different samples. The values of the mobility at room temperature are consistent with space-charge limited currents, but considerably larger than the values from transient electroluminescence measurements. This indicates that the transit times obtained by the latter method are dominated by the much lower electron mobility rather than by the hole mobility. Assuming luminescence quenching within a distance of 20 nm of the Al contact, an electron mobility of about 10^{-8} cm^2 V^{-1} s^{-1} can be estimated at room temperature and fields in the region of 10^5 V cm^{-1}.

I. Introduction

In the last two decades, the semiconducting properties of conjugated polymers have been intensively studied because of their potential applications in electronics. Field effect transistors and Schottky diodes have been fabricated from a variety of materials.[1,2] More recently, light-emitting diodes (LEDs) based on conjugated polymers have attracted considerable interest for large area displays.[3–7] Poly(*p*-phenylenevinylene) (PPV) can still be regarded as the prototype luminescent conjugated polymer and together with its many derivatives has proved to be one of the best performing materials for polymeric electroluminescent devices.[8–11] In all of these applications the transport mechanisms in the polymer layer and the nature of the contacts between the electrodes and the polymer are of great importance.

For devices based on PPV and its derivatives, both injection and bulk dominated mechanisms have been proposed as the relevant processes for the current–voltage behaviour. Parker[12] was able to fit the current–voltage characteristics of indium–tin oxide (ITO)/poly-[2-methoxy-5-(2′-ethylhexyloxy)-1,4-phenylenevinylene] (MEH-PPV)/metal devices using Fowler–Nordheim tunnelling of holes. The barrier heights obtained correspond to the difference between the work function of ITO and the ionization potential of MEH-PPV. Similar behaviour was also observed for PPV devices at higher electric fields.[13] The application of tunnelling theory for charge carrier injection assumes an insulating material with rigid energy bands forming a neutral contact with the metal electrodes. Band bending effects, *e.g.*, due to image force barrier lowering (Schottky effect), only occur within a small distance of the interface.

It has been shown recently by the Sheffield group[14] that Fowler–Nordheim tunnelling cannot satisfactorily describe their data on thin ($d \approx 100$ nm) ITO/PPV/Al devices. Although reasonable values of the hole barrier (0.3 eV) were obtained in the high field regime, the theory cannot account for the observed temperature dependence, the thickness dependence and the magnitude of the current at a given bias. Instead, they could fit their device characteristics very well by space-charge limited conduction with an exponential distribution of traps with a characteristic energy of 0.15 eV and a trap density of 5×10^{17} cm^{-3}. On the other hand, the Philips group were able to describe their current–voltage characteristics of dialkoxy-PPV based devices by space-charge limited conduction with a hopping transport mobility without the need for explicitly involving traps.[15,16]

Previous work by our group on thicker ($d > 200$ nm) ITO/PPV/Al devices has shown that a Schottky barrier with a depletion layer of width 50–150 nm is present at the Al/PPV interface.[17,18] From capacitance–voltage measurements, an acceptor dopant concentration in the order of 10^{17} cm^{-3} was determined. The occurrence of doping in PPV devices is not unexpected, since in the used precursor route to PPV the conversion of the deposited precursor polymer film to the conjugated PPV is performed at elevated temperatures directly on the electrode used for hole injection in LEDs. The precursor leaving groups (especially HCl) can easily react with the ITO

substrate forming $InCl_3$, which in turn can diffuse into the PPV layer and oxidize (dope) the polymer. The chemical reaction at the ITO substrate has been proved by energy-dispersive X-ray analysis[19] and the subsequent diffusion by secondary ion mass spectrometry (SIMS).[20] A comparison of different substrate materials has shown that the degree of doping resulting from such chemical reactions depends on the reactivity of the substrate material.[21] While PPV devices on Au substrates did not show measurable doping, in devices on ITO an acceptor dopant concentration of about 10^{17} cm^{-3} was found. Thus we could identify the usage of ITO anodes as a major source for doping in PPV devices. This doping is responsible for the formation of a Schottky contact at the interface between PPV and metals such as Ca or Al.

From this brief survey of literature data, it is obvious that within the same class of materials and even on nominally the same PPV prepared by the tetrahydrothiophene leaving group precursor route, different device characteristics are observed and described by different models. Hence, in order to compare different materials, device characteristics and their modelling, it is necessary to obtain quantitative information about the energy and concentration of gap states involved in transport and also the charge carrier mobilities. In this paper we review our recent results on devices based on PPV prepared by the precursor route which were obtained by temperature dependent impedance spectroscopy,[22] thermally stimulated currents[23] and different methods for determining charge carrier mobilities.[24,25]

II. Impedance spectroscopy

Impedance or dielectric spectroscopy is a powerful tool to study relaxation and loss processes in organic and inorganic materials, both in solution and in the solid state.[26–29] It allows one to study not only material parameters such as the frequency dependent complex dielectric constant (or equivalent the complex conductivity), but also the influence of interfaces between two different materials. The application of bias allows additional measurement techniques such as capacitance–voltage spectroscopy, which is a well established method to investigate depletion regions and the corresponding doping or trap concentrations in semiconducting materials.

For the analysis of the data it is important that there are different but equivalent impedance and admittance representations. The quantities obtained directly in impedance spectroscopy are the real and imaginary parts of the frequency dependent complex impedance:

$$\hat{Z} = \frac{d\hat{U}}{d\hat{I}} = Z' + jZ'' \tag{1}$$

Further, one has the dielectric function $\hat{\epsilon}(\omega)$ defined by

$$\hat{\epsilon} = \frac{1}{j\varepsilon_0\,\omega\hat{Z}(A/d)} = \varepsilon' + j\varepsilon'' \tag{2}$$

where ε_0 is the vacuum permittivity, d and A are the thickness and the active area of the sample, respectively, and ω is the angular frequency.

A. Temperature dependence of the dielectric function

Fig. 1 shows the spectrum of the frequency dependent dielectric function of an ITO/PPV/Al diode with a thickness $d = 700$ nm and $A = 25$ mm^2 at zero bias $U = 0$ V. The imaginary part of the dielectric function $\varepsilon''(\omega)$ shows four maxima at room temperature which have to be attributed to relaxation processes. The first of these processes lies at a frequency of about 2×10^6 Hz and is virtually independent of temperature.

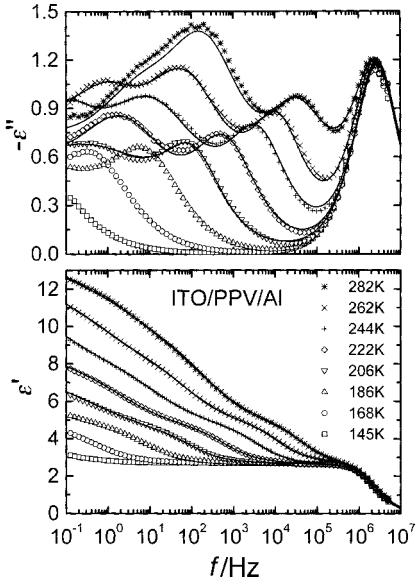

Fig. 1 (a) Imaginary and (b) real parts of the dielectric function $\hat{\epsilon}$ of an ITO/PPV/Al sample ($d = 780$ nm, $A = 25$ mm^2) at different temperatures. There exist several clearly resolved maxima in ε'', which have to be attributed to relaxation processes. These processes are more smeared out in ε', which does not achieve saturation at the lowest frequencies. The solid lines are fit curves described in the text. Reprinted with kind permission from ref. 22.

The second and third processes lie at room temperature between 2×10^4 and 3×10^5 and between 1×10^2 and 4×10^2 Hz, respectively. Both of these processes are temperature dependent; they move to lower frequencies with decreasing temperature and at low temperature they cannot be completely observed in the measured frequency window.

The real part of the dielectric function ε' decreases continuously with increasing frequency. Although one can see different relaxation processes also in ε' (*i.e.*, hints of steps), they are much more smeared out than the maxima in ε''. At 0.1 Hz ε' does not reach a saturation value in the measured temperature range. The decrease in ε' or the maximum of ε'' above 10^6 Hz is not connected with processes in the diode but arises from the no-load capacitance and the lead resistance of the diode, as will be seen below. For the explanation of the two other processes, a simple equivalent circuit consisting of a series of two parallel RC elements used in previous work[17] is not sufficient since it does not contain two thermally activated processes resulting in the observed shift with temperature. It has been shown instead that it is the inhomogeneity of the PPV bulk which gives an explanation for these processes. Hence an additional RC element ascribed to a second process in the PPV bulk is necessary to account for the observed behaviour. The corresponding equivalent circuit is shown in Fig. 2. The PPV device fabrication can lead to bulk inhomogeneity. Because PPV is insoluble, in our preparation route a prepolymer is used for film fabrication which has to be ther-

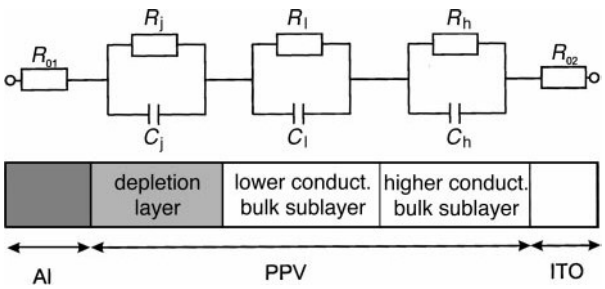

Fig. 2 Equivalent circuit used to model the behaviour of the dielectric function shown in Fig. 1.

mally converted to PPV. During the conversion, aggressive leaving groups such as HCl and tetrahydrothiophene are formed which can react with the ITO substrate to form compounds such as $InCl_3$ that can further oxidize (dope) the PPV. Since the oxidizing agents are mainly formed at the interface to ITO, it is expected that a gradient in doping will exist in the PPV film with the highest value at the ITO. Such a gradient of In and Cl is evident from the above mentioned SIMS measurements. Consequently, one cannot expect a constant conductivity profile throughout the whole PPV film.

According to the equivalent circuit shown in Fig. 2, the complex impedance is given by

$$\hat{Z} = R_0 + \sum_i \frac{1}{(1/R_i) + j\omega C_i} \tag{3}$$

Then from eqn. (2) one obtains the dielectric function as

$$\hat{\epsilon} = \left[j\omega C_{\text{geo}} R_0 + \sum_i \frac{C_{\text{geo}}}{C_i} \frac{1}{1 + (j\omega C_i R_i)^{-1}} \right]^{-1} \tag{4}$$

with $C_{\text{geo}}{}^{-1} = \Sigma_i C_i{}^{-1}$. As described in ref. 22, one can now introduce distribution parameters α_i to account for the gradual change of the conductivity profile throughout the PPV layer, leading to the following dielectric function:

$$\hat{\epsilon} = \left[(j\omega C_{\text{geo}} R_0)^{\alpha_0} + \frac{C_{\text{geo}}}{C_{\text{j}}} \frac{1}{1 + (j\omega C_{\text{j}} R_{\text{j}})^{-\alpha_{\text{j}}}} + \frac{C_{\text{geo}}}{C_{\text{l}}} \frac{1}{1 + (j\omega C_{\text{l}} R_{\text{l}})^{-\alpha_{\text{l}}}} + \frac{C_{\text{geo}}}{C_{\text{h}}} \frac{1}{1 + (j\omega C_{\text{h}} R_{\text{h}})^{-\alpha_{\text{h}}}} \right]^{-1} \tag{5}$$

This dielectric function is similar to the commonly used Cole–Cole dielectric function to describe dielectric relaxation processes in disordered media. There the distribution parameters α_i correspond to a distribution of relaxation times due to different local environments. However, in our case, it is clear that the distribution parameters α_i are caused essentially by the inhomogeneity of the PPV conductivity. As can be seen from the lines in Fig. 1, this equation yields reasonable fits over the whole temperature range. The fit parameters obtained are given in Table 1. We note that the identification of relaxation processes observed in the dielectric function with *RC* elements in an equivalent circuit such as that used here is not necessarily unique if arbitrary numbers for R_i and C_i are involved. However, as one can see from the data in Table 1, all capacitances involved are in the same range so that the position of the relaxation process on the frequency axis is simply given by the corresponding resistance and thus the assignment is unique.

The physically most important parameters from these fits are the dielectric relaxation times $\tau_i = R_i C_i$. They are connected with the dc conductivity $\tau = \varepsilon_0 \varepsilon_r / \sigma_{\text{dc}}$. Because the dc conductivity of PPV is thermally activated, we expect that the dielectric relaxation times of the two bulk processes, τ_{h} and τ_{l}, show the same behaviour. In Fig. 3 an Arrhenius plot of the bulk conductivities σ_{l} and σ_{h} calculated from the relaxation times τ_{l} and τ_{h} by $\sigma_i = \varepsilon_0 \varepsilon / \tau_i$ is presented; σ_{l} and σ_{h} correspond to the lower and higher conducting bulk sublayers,

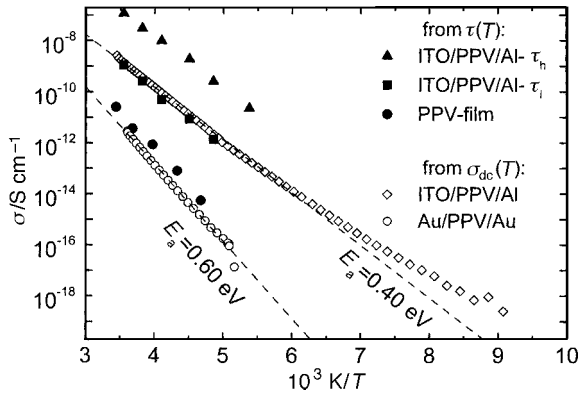

Fig. 3 Directly measured dc conductivities of an ITO/PPV/Al and a Au/PPV/Au sample in comparison with the low and high conductivities calculated from the relaxation times which are obtained from fitting the dielectric function of the ITO/PPV/Al device (of Fig. 1) and the same for a free-standing PPV film (only one relaxation process is seen in this case). Reprinted with kind permission from ref. 22.

respectively. The slope of the linear fit of ln σ_{h} *versus* $1/T$ results in an activation energy $E_{\text{a}}^{\text{h}} = 0.4$ eV. σ_{l} yields a slightly higher activation energy $E_{\text{a}}^{\text{l}} = 0.44$ eV. In Fig. 3 the temperature dependence of the conductivities for the high and low conducting regions are compared with three other independent measurements. First the same spectroscopic method is applied to a free-standing PPV film sandwiched between two gold plates. In this case only one thermally activated process (activation energy about 0.6 eV) is obtained and the value of the conductivity is much smaller. Further, for two different samples the results of direct dc conductivity measurements are given. One of them also has the ITO/PPV/Al configuration and is comparable to that in Fig. 1 and the other is an Au/PPV/Au device. The agreement between the direct dc conductivity measurements and the data calculated from the dielectric relaxation times regarding the activation energy and also the absolute numbers of the conductivity (with the value of σ_{l} calculated from τ_{l} for the ITO/PPV/Al device) is excellent. At room temperature the conductivities of the higher and lower conductive bulk sublayers are about 10^{-7} and 10^{-9} S cm^{-1}, respectively. The value 4×10^{-9} S cm^{-1} of the dc conductivity, which measures the sum of both bulk sublayer resistances and hence the mean conductivity weighted by the widths of these sublayers, is only slightly higher than σ_{l}. Both the free-standing film and the Au/PPV/Au sample have nearly the same and larger activation energy of about 0.6 eV and their conductivity at room temperature is about three orders of magnitude lower than that of PPV on ITO. Both results indicate the role of ITO in the unintentional doping process during the preparation of the ITO/PPV/Al diodes leading to an increase in the conductivity and a lowering of the activation energy to about 0.4 eV.

B. Temperature dependence of the ionized acceptor dopant concentration

In the preceding subsection we have shown that detailed information on the internal structure of the PPV layer in the

Table 1 Parameters obtained by fitting eqn. (5) to the experimental data depicted in Fig. 1

Parameter	186 K	206 K	222 K	244 K	262 K	282 K
C_{l}/nF	3.63	5.25	4.76	4.77	4.73	3.24
R_{l}/Ω	2.08×10^9	2.99×10^7	5.37×10^6	8.51×10^5	1.63×10^5	6.2×10^4
α_{l}	0.36	0.50	0.55	0.56	0.62	0.57
C_{h}/nF	2.58	2.43	2.20	2.28	2.63	2.46
R_{h}/Ω	3.63×10^6	3.45×10^5	5.25×10^4	9.06×10^3	2.59×10^3	7.79×10^2
α_{h}	0.76	0.76	0.76	0.80	0.84	0.83
C_{geo}/nF	0.76	0.77	0.78	0.71	0.74	0.80
R_0/Ω	73.24	70.81	68.13	69.15	65.00	69.80
α_0	1	1	1	0.98	0.91	0.88

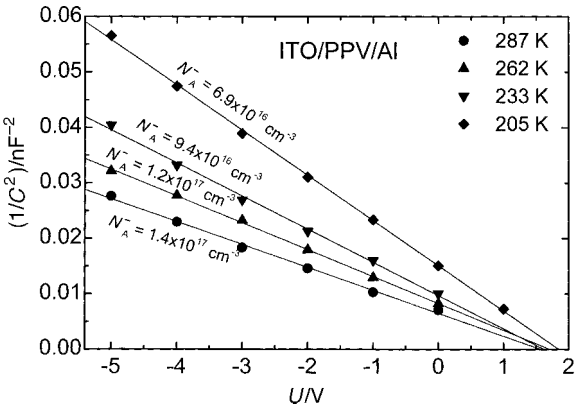

Fig. 4 The reciprocal of the square of the capacitance as a bias dependent function for an ITO/PPV/Al sample (d = 600 nm, A = 25 mm^2) measured at 0.16 Hz at different temperatures. The acceptor dopant concentration is obtained from linear fits according to eqn. (4) between −5 and 1 V. Reprinted with kind permission from ref. 22.

diodes can be obtained by appropriately analysing the data from dielectric impedance spectroscopy. More common for semiconductor/metal contacts is the measurement of the bias dependent capacitance of the depletion layer C_j. Under the assumption that at reverse bias the depletion layer resistance is much larger than the serial bulk resistances, the junction capacitance C_j is approximately the total measured low frequency parallel capacitance. For an abrupt junction the depletion layer capacitance of a Schottky contact is given by[30]

$$C_j = A\sqrt{\frac{q\varepsilon_0\,\varepsilon_r\,N_A^-}{2(U_D - U)}} \tag{6}$$

where N_A^- is the ionized acceptor concentration and U_D the diffusion voltage. Thus a linear plot of $1/C_j^2$ *versus* bias voltage should give a straight line with a slope proportional to $1/N_A^-$.

Fig. 4 shows the reciprocal of the square of the junction capacitance of an ITO/PPV/Al sample (d = 600 nm) measured at 0.16 Hz as a bias-dependent function for various temperatures. Here the linear behavior of $1/C_j^2$ *versus* bias voltage in the reverse direction is clearly seen. This means that the concept of a simple Schottky junction at the interface can be applied to this device. All linear fits in Fig. 4 give a value of about 1.5–1.7 V for the diffusion voltage, which is comparable to our earlier results.[17] In principle, one would expect to see a reduction in the diffusion voltage with decreasing temperature as the reduced effective dopant concentration leads to an increased work function of the polymer. However, we note that the determination of the diffusion voltage from the intercept with the abscissa can be affected by several factors such as bulk resistance or capacitance, leading to offsets of the data on the voltage or capacitance axis. Additionally, since the data were obtained from frequency dependent measurements at fixed bias, as opposed to bias dependent measurements at fixed frequency, we do not have enough data in the vicinity of the diffusion voltage to make decisive statements about the temperature dependence of the diffusion voltage. Nevertheless, the tendency of the temperature dependence of N_A^- is significant: with decreasing temperature (from 287 to 205 K) N_A^- decreases from 1.4×10^{17} to 6.9×10^{16} cm^{-3}. The corresponding depletion layer width at zero bias increases from about 55 nm at room temperature to about 80 nm at 205 K.

One can obtain the temperature dependence of the ionized acceptor concentration as in conventional semiconductors from

$$N_A^- = -\frac{1}{2}N_V \exp\left(-\frac{E_A}{k_B T}\right)\left[1 - \sqrt{1 + 4\frac{N_A}{N_V}\exp\left(\frac{E_A}{k_B T}\right)}\right] \tag{7}$$

where E_A is the acceptor ionization energy, N_V the effective density of states in the valence band and N_A the density of electrically active acceptors. For the sample shown in Fig. 4 we have the values for the density of ionized acceptors $N_A^-(T)$ presented in Fig. 5. It should be noted that C_j of all our samples does not saturate at room temperature. This means that the condition of complete acceptor ionization at room temperature is not sufficiently fulfilled. Nevertheless, assuming $N_A^- \approx 90\%$ of N_A at room temperature, one can try to fit eqn. (7) to the calculated data for $N_A^-(T)$ shown in Fig. 5. With $N_V = 5 \times 10^{21}$ and 5×10^{20} cm^{-3},[31,32] this fit yields E_A = 0.2 and 0.16 eV, respectively. Such low values are in contrast to the activation energy obtained from direct dc conductivity measurements and the relaxation times from impedance spectroscopy (E_a = 0.4 eV). However, the data cannot be fitted using E_A = 0.4 eV and $N_V = 10^{21}$ cm^{-3}: for these parameters N_A^- is only 2% of N_A at room temperature. From our data, one has to conclude that the characteristic energies responsible for the transport in the PPV bulk (with E_a = 0.4 eV for ITO substrates) and the temperature dependent behaviour of the depletion layer (leading to an acceptor energy E_A = 0.16–0.2 eV) are significantly different. So far in dc conductivity measurements by our group and others, activation energies between 0.4 and 0.9 eV[33–35] (depending on the substrate and environmental conditions) have been found with no indication of acceptor states with energies lower than 0.2 eV.

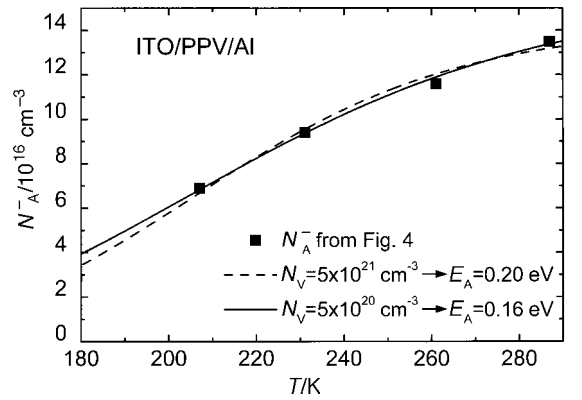

Fig. 5 Temperature dependence of the ionized acceptor concentration for the sample in Fig. 4 and fits with eqn. (5) using two different densities of valence band states. Reprinted with kind permission from ref. 22.

III. Thermally stimulated currents

In order to obtain independent information about the energy and density of gap states, we performed thermally stimulated current (TSC) measurements on PPV LED structures. The method of TSC has been widely used to determine the density and energy distribution of trap states in inorganic semiconductors, organic molecular crystals and polymeric photoconductors.[36–39] The experiment consists of filling the trap states at low temperature either by passing a current through the sample or by photoexcitation, then heating the sample in the dark at a constant rate with or without an external field. As the traps are released a current is measured and characteristic peaks are observed. By integrating the released current over time, the amount of trapped charges is obtained and knowing the volume of the sample one can estimate the average trap density. If the specimen is heated at a constant rate $\beta = \mathrm{d}T/\mathrm{d}t$ the measured current due to detrapping of car-

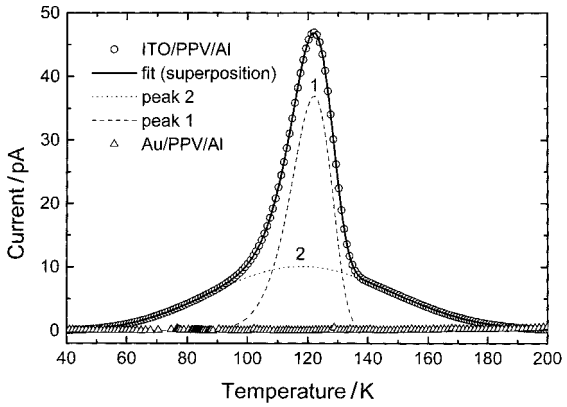

Fig. 6 Comparison of TSC spectra of an ITO/PPV/Al and a Au/PPV/Al device. Both samples were measured simultaneously after identical trap filling. The spectrum of the ITO device can be fitted by a superposition of two peaks. Reprinted with kind permission from ref. 23.

riers is given by[40,41]

$$I(T) \propto n_{t_0} \exp\left[-\frac{E_t}{kT} - \int_{T_0}^{T} \frac{\nu}{\beta} \exp\left(-\frac{E_t}{kT'}\right) dT'\right] \quad (8)$$

where n_{t_0} denotes the density of filled traps at the initial temperature T_0, E_t the trap depth and ν the attempt-to-escape frequency.

In order to determine the density and energy levels of states created by the chemical reaction of the PPV precursor leaving groups with the substrate, we performed TSC measurements on devices with different anodes. Fig. 6 shows a comparison of TSC spectra of ITO/PPV/Al and Au/PPV/Al devices in the temperature range from 40 to 200 K. Both samples had a PPV layer thickness of about 600 nm with an active area of 0.25 cm^2 and the trap filling was performed identically, passing a current of 10 μA at 10 K for 5 min through the device in forward bias direction (ITO positive). The curves were recorded in the short circuit mode (without an externally applied field) at a heating rate of about 5 K min^{-1}. Whereas there is no TSC signal detectable within our experimental resolution (10^{-13} A) when Au is used as the anode, the sample with ITO clearly shows a peak at about 122 K. In several measurement cycles we confirmed that this peak only occurred when the traps were filled prior to heating the sample. Thus, the elimination of PPV on ITO substrates creates at least one trap state in the polymer which can be detected with TSC. The TSC spectrum of the ITO sample was fitted by a superposition of two TSC peaks as shown by the solid line in Fig. 6. The least squares fit gives a trap depth of $\Delta E = 0.18$ eV ($T_{max} = 122$ K) for the narrow peak 1. For the second underlying broader peak 2 a trap depth of about $\Delta E = 0.03$ eV is obtained. The values vary from sample to

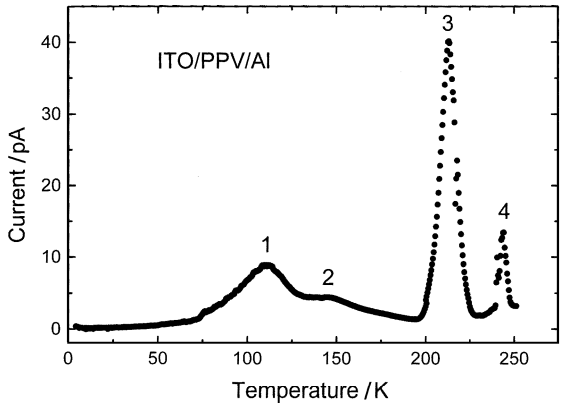

Fig. 7 Complete TSC spectrum of an ITO/PPV/Al device between 50 and 200 K (PPV converted in Ar atmosphere). Reprinted with kind permission from ref. 23.

sample typically between 0.03 and 0.05 eV for peak 2 and between 0.13 and 0.18 eV for peak 1. The integral of the TSC current $I(t)$ over time t yields the amount of detrapped charges Q_t. If all traps are filled at low temperature the integral gives the density of releasable traps. Q_t saturates at a level of 25×10^{-9} C, which corresponds to an average density of releasable traps of $n_t = 1.2 \times 10^{16}$ cm^{-3}. This is in the same range as the dopant concentration N_A^- which we have obtained from the capacitance–voltage measurements discussed before. These numbers suggest that the ITO related trap states are responsible for the p-type doping of PPV and hence for the observed Schottky-diode behaviour of ITO/PPV/metal LEDs. In the case of the Au devices no such peak structure is observable in this temperature range, which correlates well with the absence of a voltage dependent capacitance and an increased bulk resistance of the LEDs with an Au anode. The dopant concentration in PPV converted on Au is estimated to be below 10^{15} cm^{-3}.[21]

In the TSC spectrum in Fig. 6 data were plotted only up to a temperature of 200 K. Between 200 and 300 K further peaks appear in the spectra independent of the chosen anode substrates. As an example, we show in Fig. 7 the complete TSC spectrum of an ITO/PPV/Al device between 5 and 250 K. In addition to the already discussed peaks originating from the reaction with the ITO substrate (peaks 1 and 2), there are two narrow peaks in the temperature range above 200 K. The corresponding trap energies are about 0.9 and 1.0 eV for peaks 3 and 4, respectively. We have found that the relative peak height, width and position can vary from sample to sample and also depend on the device history. For the trap energies, values between 0.6 and 0.9 eV for peak 3 and between 0.9 and 1.0 eV for peak 4 have been obtained. These energies are similar to the activation energy obtained from temperature dependent conductivity measurements as discussed before. The small width of the TSC peaks 3 and 4 in Fig. 7 indicates the existence of distinct trap levels. Nevertheless, a distribution of trap states cannot be fully excluded. However, the data analysis used here does not allow us to make a quantitative estimate of the width of the distribution. We note that such deep trap states in PPV LEDs have recently been measured independently by using deep level transient spectroscopy.[42] Trap depths of 0.8 eV and densities of 4×10^{16} cm^{-3} were found.

Our investigations have shown that the density of these deeper states depends on the degree of exposure to air. The trap density can be reversibly reduced below 10^{15} cm^{-3} or enhanced to 10^{17} cm^{-3} by keeping the sample in vacuum or ambient conditions. Thus we have evidence that a reversible doping process by one or more components of air is responsible for these deep states. Since reversible doping effects by atmospheric oxygen have been reported for several conjugated polymers (see, *e.g.*, ref. 43), it is very likely that the diffusion of molecular oxygen into the polymer and the subsequent formation of polarons by a structural distortion of the polymer chain are also responsible for the reversible doping observed in PPV.

IV. Charge carrier mobility

Charge carrier mobilities were studied by the time-of-flight (TOF) technique for two soluble PPV derivatives.[44,45] However, up to now the drift mobility could not be directly measured in unsubstituted PPV because of a featureless photocurrent decay. From their data, Meyer *et al.*[45] could only estimate an upper limit for the hole mobility of less than 10^{-8} cm^2 V^{-1} s^{-1}. Therefore, our work was aimed primarily at the direct determination of the drift mobility of carriers in PPV and the investigation of the temperature and field dependent characteristics of the mobility. In this paper, we present results on the hole mobility in unsubstituted PPV obtained by

the classical TOF method and compare these data with results from space-charge limited currents and transient electroluminescence.

A. Time-of-flight measurements

The standard method to obtain charge carrier mobilities in insulating materials is to measure the transit time of excess carriers generated close to one electrode to reach the counter electrode. In the conventional TOF method these carriers are generated by illumination with a short ultraviolet light pulse. Depending on the polarity of the electric field, only one type of carrier will be accelerated towards the counter electrode. Electrical injection by the contacts has to be excluded in this experiment. For ITO/PPV/Al devices this has as a consequence that the illumination through the transparent ITO contact is not possible when the hole mobility is to be determined. Instead, a semitransparent Al contact has to be used.

In the following we discuss only briefly the results on the hole mobility in PPV obtained by TOF, since a detailed analysis has been published recently.[24,25] Fig. 8 shows a typical photocurrent transient of holes in PPV. The structureless decay in a linear representation (see the inset) is typical for dispersive transport in a large class of amorphous polymers.[46] The transit time t_T can only be obtained from the change of slope in a double logarithmic plot. The drift mobility can then be calculated as

$$\mu = \frac{d^2}{t_T V} \tag{9}$$

where d is the thickness of the sample and V the applied voltage. The value calculated from the data in Fig. 8 is $\mu = 1.4 \times 10^{-5}$ cm^2 V^{-1} s^{-1}. We note that photocurrent transients with a clearly detectable transit time could only be observed on samples, where the film casting and thermal conversion was performed in several steps as described in ref. 24. Thick films converted in only one conversion step did not show this feature. Hence our improved film preparation technique is necessary for obtaining hole mobilities in PPV directly by TOF. However, even with this improved preparation method we have not been able to determine transit times of electrons in PPV. This is probably due to severe trapping observed before by measuring $\mu\tau$ products with TOF[47] and also from trap limited conduction seen in the current–voltage characteristics of Ca/dialkoxy-PPV/Ca electron-only devices.[48]

TOF measurements were performed in the temperature range between 275 and 320 K and applied electric fields between 6.4×10^4 and 4×10^5 V cm^{-1}. The mobility obtained follows an Arrhenius law with a field dependent activation energy as shown in Fig. 9. The activation energy E_A

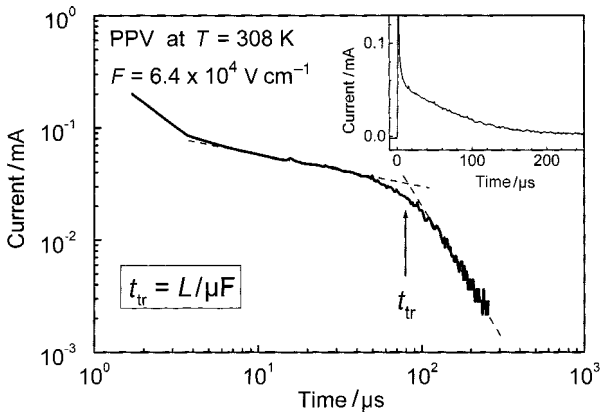

Fig. 8 Photocurrent transient of holes in an ITO/PPV/Al device at a temperature $T = 308$ K and an electric field $F = 6.4 \times 10^4$ V cm^{-1} in a linear (inset) and in a double logarithmic representation. The PPV thickness was 0.7 μm. Reprinted with kind permission from ref. 24.

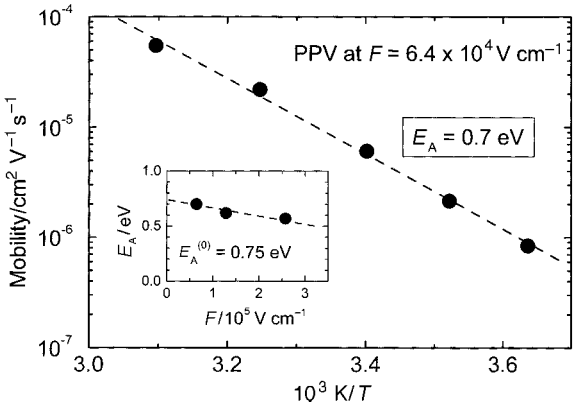

Fig. 9 Temperature dependence of the drift mobility in PPV at $F = 6.4 \times 10^4$ V cm^{-1} in an Arrhenius representation. The inset shows the field dependent activation energy of the drift mobility with an extrapolation to zero field. Reprinted with kind permission from ref. 24.

decreases with increasing field and the extrapolation gives a rough estimate of $E_A^{(0)} = 0.75$ eV at zero field (inset in Fig. 9). This value is in the same range as the measured activation energy of the dc conductivity of PPV. We note that the activation energy varies from sample to sample between 0.4 and 0.7 eV. However, as impedance spectroscopic investigations and thermally stimulated currents indicate, in PPV there are at least two sets of gap states with energies in the ranges 0.05–0.2 and 0.6–1 eV, respectively. The combination of these different states with varying density may explain the variations of the activation energy from sample to sample.

The field dependence of the drift mobility at $T = 277$ K is presented in Fig. 10. The drift mobility of the positive charge carriers increases with increasing electric field. In both representations linear regressions yield satisfactory fits of the experimental data. It is therefore hard to distinguish whether a polaron hopping model[49] (a) or a Poole–Frenkel mechanism (b) is more appropriate to describe the measured mobility of PPV.

Compared with the soluble PPV derivatives, the mobility data for PPV are in the same order of magnitude as with a phenyl-substituted PPV (PPPV)[44] and only about a factor of 10 lower than in diphenoxyphenyl-PPV (DPOP-PPV),[45] indicating that the precursor route to PPV does not necessarily produce films with higher defect concentrations and reduced carrier mobility.

B. Space-charge limited currents

Another method which is frequently used to obtain charge carrier mobilities is the observation of space-charge limited currents (SCLC) in current–voltage characteristics. In the trap-free case the current–voltage characteristics should follow

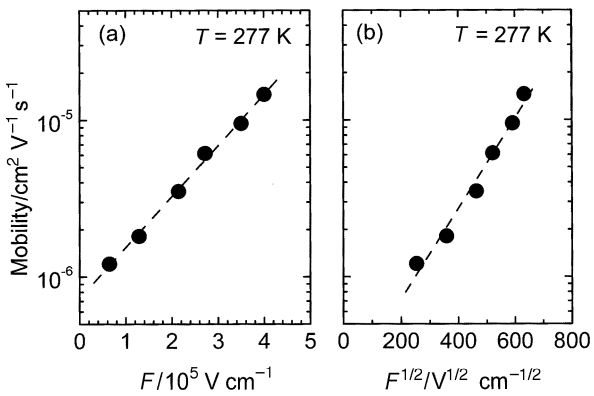

Fig. 10 Dependence of the drift mobility in PPV at $T = 277$ K on (a) the electric field (polaron hopping model) and (b) the square root of the electric field (Poole–Frenkel model). Reprinted with kind permission from ref. 24.

Child's law with

$$j = \frac{9}{8}\epsilon_0 \epsilon_r \mu \frac{V^2}{d^3} \quad (10)$$

which allows for a direct determination of the effective carrier mobility μ. This method was succesfully applied to hole transport in dialkoxy-PPV by Blom *et al.*[15,16,48] Assuming a Poole–Frenkel-like field dependence of the mobility, they could fit their data at room temperature up to fields of 3×10^5 V cm^{-1} with a zero-field mobility of 5×10^{-7} cm^2 V^{-1} s^{-1} From temperature dependent measurements, an activation energy of about 0.5 eV was obtained.

In order to identify SCLC, one usually plots the current–voltage characteristics in a double-logarithmic representation, where Child's law yields a straight line with a slope of two. Fig. 11 shows an *I–V* curve for an ITO/PPV/Al device (thickness 600 nm, area 0.14 cm^2) in the forward bias direction. Data were taken in the dc mode up to 5 V; above that value up to 80 V a pulse technique was used. The solid line indicates a power law with a slope of 2.5, which is larger than predicted by Child's law. Regarding the field dependent mobility obtained from the TOF measurements, however, this steeper increase is understandable, since the mobility should increase with increasing field. Strictly, eqn. (10) is no longer valid in this case. The dashed line indicates the value of the current that would be expected for Child's law with a hole mobility of 8×10^{-5} cm^2 V^{-1} s^{-1}, which is in a reasonable range regarding the TOF mobility data.

C. Transient electroluminescence

It was shown by Karg *et al.*[50] that the presence of a Schottky contact in our ITO/PPV/Al devices with a depletion layer of width between 50 and 100 nm can be utilized to obtain information on the charge carrier mobility from transient electroluminescence (EL) measurements. The delay time between the rising edge of the voltage pulse and the first appearance of EL is in general determined by both the hole and electron mobility:

$$t_d = \frac{d}{(\mu_h + \mu_e)F} \quad (11)$$

Assuming that the delay time is solely determined by the transit of holes through the depletion layer at the Al contact, mobilities of about 10^{-7} cm^2 V^{-1} s^{-1} at a field of 2×10^5 V cm^{-1} have been obtained at room temperature. The data are shown in Fig. 12 as a function of the square root of the electric field. These values are about two orders of magnitude lower than the TOF results. One important reason for this discrepancy is that the contribution of the electron motion to the delay time was neglected since the electron mobility in

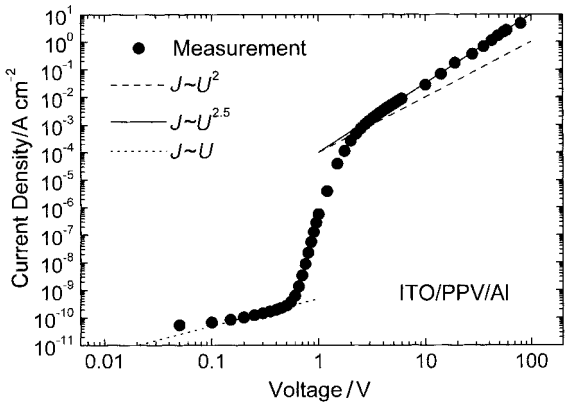

Fig. 11 Current–voltage characteristics of an ITO/PPV/Al device in a double-logarithmic representation. The straight lines indicate power laws with different exponents. The dashed line was calculated from Child's law using a mobility of 8×10^{-5} cm^2 V^{-1} s^{-1}.

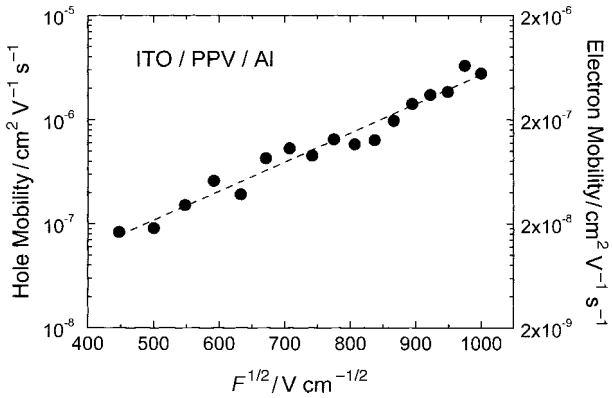

Fig. 12 Charge carrier mobilities calculated from the delay time in transient electroluminescence measurements. Left-hand axis: hole mobilities obtained by assuming recombination directly at the electrode. Right-hand axis: electron mobilities calculated from the same data taking into account luminescence quenching at the cathode.

PPV and its derivatives was estimated to be several orders of magnitude lower than the hole mobility.[47,48] This assumption implies that electron–hole or exciton recombination takes place directly at the Al contact. However, it is known from organic single crystals[51] and also was recently shown for polymeric light-emitting devices[52] that the presence of the metal electrode quenches EL within a distance of 15–20 nm from the electrode. Recent measurements of photoluminescence quenching in PPV in the presence of metal electrodes have indicated even larger distances (up to 60 nm) where excitation quenching plays a role.[53] Hence the contribution of electron motion to the transit time cannot be neglected.

Assuming a minimum distance of $d = 20$ nm required for the electron to avoid EL quenching (instead of $d = 100$ nm for the drift of holes through the depletion layer), the data in Ref. 48 yield an electron mobility of about 10^{-8} cm^2 V^{-1} s^{-1} at the above mentioned field. The electron mobilities calculated from the original data under this assumption are given in Fig. 12 on the right-hand axis. The low values of the electron mobility seem not unreasonable since it was estimated to be much lower than the hole mobility in other experiments.[47,48] Thus, instead of the hole mobility, in transient EL measurements one gains information about the electron mobility in PPV. In order for the delay time of EL to be dominated by hole transport, the ratio between the width of the EL quenching zone and the depletion layer (or the sample thickness) had to be much larger than the ratio of the hole to the electron mobility.

We note that other explanations for the origin of delay times in transient EL have recently been given. One is the build-up of interfacial charge densities and the concomitant redistribution of the electric field inside the device.[54] However, the system under consideration in that work was a bilayer system with relatively high electron mobilities in the electron transporting layer (which was one requirement for the model). Hence the model is probably not applicable for the case of PPV with such low electron mobilities. Generally, the identification of delay times in transient EL with charge carrier mobilities is not straightforward and has to be checked in each individual case.

V. Conclusion

The role of doping and trap states for charge carrier transport in light-emitting devices based on unsubstituted PPV has been investigated by temperature dependent impedance spectroscopy and thermally stimulated currents. It was found that the conversion of PPV on ITO substrates creates shallow traps with a depth of about 0.1–0.2 eV, which are responsible for the p-type doping of PPV and govern the room temperature device characteristics. The total density of ionized acceptors at

room temperature is of the order of 10^{16}–10^{17} cm^{-3}. The temperature dependent behaviour of electrical transport quantities such as conductivity and mobility is dominated by deeper states with energies in the range 0.6–1 eV. Their density can be varied by applying a vacuum to the devices.

The mobility of positive carriers in PPV has been determined by the TOF method in the region of 10^{-5} cm^2 V^{-1} s^{-1} at room temperature for an electric field of about 10^5 V cm^{-1}. Field and temperature dependent TOF measurements yield an exponential increase in the mobility with the applied field and thermally activated behaviour with activation energies between 0.4 and 0.7 eV on different samples. The values of the mobility at room temperature are consistent with space-charge limited currents, but considerably larger than the data from transient electroluminescence measurements. This indicates that the transit times obtained by the latter method are dominated by the much lower electron mobility rather than by the hole mobility.

Acknowledgements

We thank M. Meier, J. Scherbel, K. Zuleeg, S. Karg, T. Dittrich, E. Lebedev and G. Paasch for their contributions to parts of this work and J. Gmeiner for polymer synthesis. Financial support from the Bayerische Forschungsstiftung (FOROPTO) is gratefully acknowledged.

References

1 J. Kanicki, in *Handbook of Conducting Polymers*, ed. T. A. Skotheim, Marcel Dekker, New York, 1986, p. 543.
2 J. H. Burroughes, C. A. Jones and R. H. Friend, *Nature (London)*, 1988, **335**, 137.
3 J. H. Burroughes, D. D. C. Bradley, A. R. Brown, R. N. Mackay, R. H. Friend, P. L. Burn and A. B. Holmes, *Nature (London)*, 1990, **347**, 539.
4 D. Braun and A. J. Heeger, *Appl. Phys. Lett.*, 1991, **58**, 1982.
5 D. D. C. Bradley, *Synth. Met.*, 1993, **54**, 401.
6 N. C. Greenham and R. H. Friend, in *Solid State Physics*, ed. H. Ehrenreich and F. Spaepen, Academic Press, Boston, 1995, vol. 49, p. 2.
7 W. Riess, in *Organic Electroluminescent Materials and Devices*, ed. S. Miyata and H. Nalwa, Gordon and Breach, London, 199, p. 73.
8 R. H. Friend, N. C. Greenham, in *Handbook of Conducting Polymers*, ed. T. A. Skotheim, R. L. Elsenbaumer and J. R. Reynolds, Marcel Dekker, New York, 2nd edn., 1998, p. 823.
9 C. Liedenbaum, Y. Croonen, P. van de Weijer, J. Vleggaar and H. Schoo, *Synth. Met.*, 1997, **91**, 109.
10 J. C. Carter, I. Grizzi, S. K. Heeks, D. J. Lacey, S. G. Latham, P. G. May, O. Ruiz de los Panos, K. Pichler, C. R. Towns and H. F. Wittmann, *Appl. Phys. Lett.*, 1997, **71**, 34.
11 N. Tesler, N. T. Harrison and R. H. Friend, *Adv. Mater.*, 1998, **10**, 64.
12 I. D. Parker, *J. Appl. Phys.*, 1994, **75**, 1656.
13 R. N. Marks, D. D. C. Bradley, R. W. Jackson, P. L. Burn and A. B. Holmes, *Synth. Met.*, 1993, **55**, 4128.
14 A. J. Campbell, D. D. C. Bradley and D. G. Lidzey, *J. Appl. Phys.*, 1997, **82**, 6326.
15 P. W. M. Blom, M. J. M. de Jong and M. G. van Munster, *Phys. Rev. B*, 1997, **55**, R656.
16 P. W. M. Blom and M. J. M. de Jong, *IEEE J. Sel. Top. Quantum Electron*, 1998, **4**, 105.
17 M. Meier, S. Karg and W. Riess, *J. Appl. Phys.*, 1997, **82**, 1961.
18 S. Karg, M. Meier and W. Riess, *J. Appl. Phys.*, 1997, **82**, 1951.
19 M. Herold, J. Gmeiner, C. Drummer and M. Schwoerer, *J. Mater. Sci.*, 1997, **32**, 5709.
20 G. Sauer, M. Kilo, M. Hund, A. Wokaun, S. Karg, M. Meier, W. Riess, M. Schwoerer, H. Suzuki, J. Simmerer, H. Meyer and D. Haarer, *Fresenius' J. Anal. Chem.*, 1996, **353**, 642.
21 W. Brütting, M. Meier, M. Herold, S. Karg and M. Schwoerer, *Chem. Phys.*, 1998, **227**, 243.
22 J. Scherbel, P. H. Nguyen, G. Paasch, W. Brütting and M. Schwoerer, *J. Appl. Phys.*, 1998, **83**, 5045.
23 M. Meier, S. Karg, K. Zuleeg, W. Brütting and M. Schwoerer, *J. Appl. Phys.*, 1998, **84**, 87.
24 E. Lebedev, T. Dittrich, V. Petrova-Koch, S. Karg and W. Brütting, *Appl. Phys. Lett.*, 1997, **71**, 2686.
25 W. Brütting, E. Lebedev, S. Karg, T. Dittrich, V. Petrova-Koch and M. Schwoerer, *Proc. SPIE*, 1998, **3281**, 257.
26 J. R. MacDonald, *Impedance Spectroscopy*, Wiley, New York, 1987.
27 P. Blood and J. W. Orton, *The Electrical Characterization of Semiconductors: Majority Carriers and Electron States Techniques of Physics*, Academic Press, London, 1992.
28 C. J. F. Böttcher and P. Bordewijk, *Theory of Electric Polarization*, Elsevier, Amsterdam, 1978, vols. 1 and 2.
29 A. K. Johnscher, *Dielectric Relaxation in Solids*, Chelsea Dielectrics, London, 1983.
30 S. M. Sze, *Physics of Semiconductor Devices*, Wiley, New York, 1981.
31 P. S. Davids, A. Saxena and D. L. Smith, *J. Appl. Phys.*, 1985, **78**, 4244.
32 G. Paasch, P. H. Nguyen and S.-L. Drechsler, *Synth. Met.*, 1998, **97**, 255.
33 T. P. Nguyen and V. H. Tran, *Mater. Sci. Eng. B*, 1995, **31**, 255.
34 J. Gmeiner, S. Karg, M. Meier, W. Riess, P. Strohriegl and M. Schwoerer, *Acta Polym.*, 1993, **44**, 201.
35 G. Paasch, W. Riess, S. Karg, M. Meier and M. Schwoerer, *Synth. Met.*, 1994, **67**, 177.
36 J. Slowik, *J. Appl. Phys.*, 1976, **47**, 2982.
37 R. Eiermann, W. Hofberger and H. Bässler, *J. Non-Cryst. Solids*, 1978, **28**, 415.
38 I. Glowacki and J. Ulanski, *J. Appl. Phys.*, 1995, **78**, 1995.
39 E. Fabre and R. N. Bhargava, *Appl. Phys. Lett.*, 1974, **24**, 322.
40 R. Haering and E. N. Adams, *Phys. Rev.*, 1960, **117**, 451.
41 T. Cowell and J. Woods, *Br. J. Appl. Phys.*, 1967, **18**, 1045.
42 A. J. Campbell, W. S. Weaver, D. G. Lidzey, D. D. C. Bradley, E. Werner, W. Brütting and M. Schwoerer, *Proc. SPIE*, 1998, **3476**, 98.
43 D. M. Taylor, H. Gomes, A. E. Underhill, S. Edge and P. I. Clemenson, *J. Phys. D: Appl. Phys.*, 1991, **24**, 2032.
44 M. Gailberger and H. Bässler, *Phys. Rev. B*, 1991, **44**, 8643.
45 H. Meyer, D. Haarer, N. Naarmann and H. H. Hörhold, *Phys. Rev. B*, 1995, **52**, 2587.
46 P. M. Borsenberger and D. S. Weiss, *Organic Photoreceptors for Imaging Systems*, Marcel Dekker, New York, 1993.
47 H. Antoniadis, M. A. Abkowitz and B. R. Hsieh, *Appl. Phys. Lett.*, 1994, **65**, 2030.
48 P. W. M. Blom, M. J. M. de Jong and J. J. M. Vleggar, *Appl. Phys. Lett.*, 1996, **68**, 3308.
49 D. Emin, in *Electronic and Structural Properties of Amorphous Semiconductors*, ed. P. G. Lecomber and J. Mort, Academic Press, New York, 1973.
50 S. Karg, V. Dyakonov, M. Meier, W. Riess and G. Paasch, *Synth. Met.*, 1994, **67**, 165.
51 H. Kurzcewska and H. Bässler, *J. Lumin.*, 1977, **15**, 261.
52 J. Grüner, M. Remmers and D. Neher, *Adv. Mater.*, 1997, **9**, 964.
53 H. Becker, S. E. Burns and R. H. Friend, *Phys. Rev. B*, 1997, **56**, 1893.
54 V. R. Nikitenko, Y.-H. Tak and H. Bässler, *J. Appl. Phys.*, 1998, **84**, 2334.